Langevin and Trap-Assisted Recombination in Phosphorescent Organic Light Emitting Diodes

*Jeong-Hwan Lee, Sunghun Lee, Seung-Jun Yoo, Kwon-Hyeon Kim, and Jang-Joo Kim**

Bimolecular and trap-assisted recombination mechanisms are investigated in small molecule-based phosphorescent organic light emitting diodes (PhOLEDs) using the current–voltage–luminance characteristics in the diffusion current region, along with transient electroluminescence and capacitance measurements. Two different PhOLEDs, one with a single host, 4,4′-Bis(carbazol-9-yl)biphenyl, and the other with an exciplex-forming co-host, are studied. Trap-assisted recombination with a large number of trapped charges is dominant in the PhOLED with the single host because of the large energy gap between the host and the dopant state. In contrast, bimolecular Langevin recombination is dominant in the PhOLED with the exciplex forming co-host, where a phosphorescent dye is doped in the co-host. As a result, the accumulated charge density is lower in the co-host system than in the single host emission layer, leading to high efficiency that approaches the theoretical limit, with an extremely low efficiency roll-off.

1. Introduction

Understanding of the charge carrier recombination process and the emission of photons from excitons is of great importance to organic light emitting diodes (OLEDs), because it is intimately related to the performance of the devices. Under electrical excitation in phosphorescent dye-doped OLEDs (PhOLEDs), two different recombination and emission paths are available in the emission layer (EML). The first path is the formation of excitons on the host material, followed by energy transfer to the dopant via the Förster and/or Dexter mechanisms. The other path is direct recombination on the dopant via charge carrier trapping. The former is related to bimolecular recombination, i.e. Langevin recombination,[1] while the latter is trap-assisted recombination.[2,3] These two mechanisms are mutually competitive under electrical excitation in PhOLEDs and it is difficult to determine which mechanism is dominant under electrical excitation, although the determination of the mechanism may provide a critical clue toward the realization of high performance PhOLEDs. Recently, M. Kuik et al. reported the recombination and emission mechanisms in polymer LEDs based on various conjugated polymers.[4,5] The conjugated polymers contain intrinsic electron traps so that the current was governed by trap-assisted recombination, but the photons were emitted via a Langevin type emission mechanism. Unfortunately, little fundamental research has been undertaken into this issue in PhOLEDs. It has been reported that phosphorescent dopants accelerate the trapping of holes because the dopants function as hole traps within a host layer in many cases. Therefore, it brings the dominance of trap-assisted recombination to PhOLEDs under electrical excitation, resulting in efficiency enhancement of PhOLEDs.[6–13] However, energy transfer mechanism from host to dopant is too crucial to be ignored in terms of the efficiency enhancement of PhOLEDs.[10,14–17] For example, we recently reported green PhOLEDs with an almost ideal level of efficiency in terms of the external quantum efficiency (EQE), driving voltage and efficiency roll-off, with a maximum EQE of 29.1%, a turn-on voltage of 2.4 V and EQE of over 27% at 10 000 cd m^{-2}, using an exciplex forming co-host. The excellent performance of the PhOLEDs was attributed to the formation of the exciplex in the host followed by energy transfer to the dopant.[18,19] The proposed mechanism is markedly different from the trap-assisted recombination mechanism that is prevalent in most PhOLEDs reported to date.

In the present study, we clarified the charge recombination mechanisms in two different PhOLEDs: one with the exciplex forming co-host,[18,19] and the other with a single host, that is, 4,4'-Bis(carbazol-9-yl)biphenyl (CBP).[20,21] (Detailed information is shown in **Figure 1**.) The charge recombination, accumulation and light emission mechanisms were analyzed using the current density-voltage-luminance (*J*–*V*–*L*) characteristics of the devices in the diffusion current region, along with transient electroluminescence (EL) and capacitance-voltage (*C*–*V*) measurements. The results clearly showed that excitons are predominantly generated by Langevin recombination in the exciplex forming co-host, in contrast to the trap-assisted recombination on the emitter in the CBP-based PhOLED. Also, the trapped charge density in the PhOLED with the exciplex forming co-host system was lower than that in the CBP-based PhOLED. These results indicated that the exciplex forming co-host boosts the recombination of the charge carriers in the host by Langevin recombination and boosts the light emission from the emitter through energy transfer from the host rather than by trap-assisted recombination, even in the high current region. Low charge density in the PhOLEDs with the exciplex forming

Dr. J.-H. Lee, Dr. S. Lee, S.-J. Yoo,
K.-H. Kim, Prof. J.-J. Kim
Department of Materials Science and Engineering
Seoul National University
Seoul 151–744, Korea
E-mail: jjkim@snu.ac.kr

DOI: 10.1002/adfm.201303453

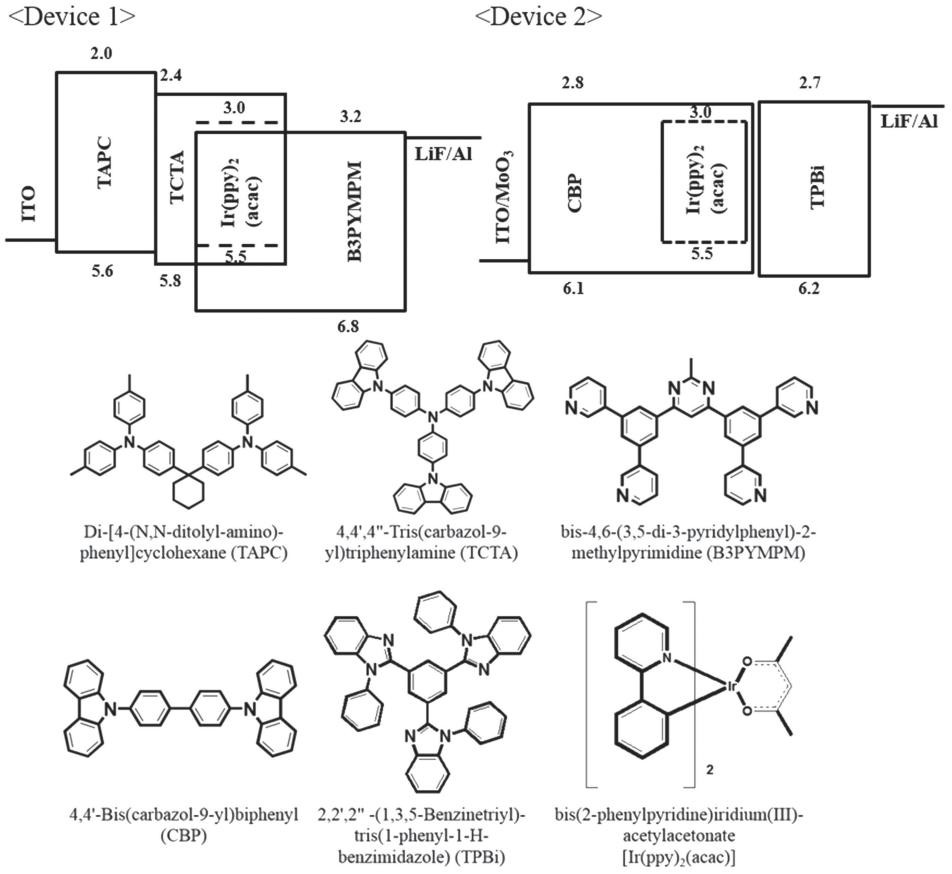

Figure 1. Device structures, the energy levels of each layer, and the molecular structures of the two different phosphorescent organic light emitting diodes (PhOLEDs).

host must be related to the low efficiency roll-off caused by reduced exciton-polaron quenching.[22–25]

2. Results and Discussions

2.1. Device Performance of the Green PhOLEDs

Figure 2 shows the *J–V–L* and external quantum efficiency–luminance characteristics of the two PhOLEDs. The structure of device 1 is indium tin oxide (ITO) (70 nm)/di-[4-(N,N-ditolyl-amino)-phenyl]cyclohexane (TAPC) (75 nm)/4,4′,4″-Tris(carbazol-9-yl)triphenylamine (TCTA) (10 nm)/TCTA:bis-4,6-(3,5-di-3-pyridylphenyl)-2-methylpyrimidine (B3PYMPM):bis(2-phenylpyridine)iridium(III)-acetylacetonate [$Ir(ppy)_2(acac)$] (1:1 molar ratio and 8 wt%, 30 nm)/B3PYMPM (40 nm)/LiF (0.7 nm)/Al (100 nm), and device 2 is composed of ITO (70 nm)/molybdenum trioxide (MoO_3) (1 nm)/CBP (90 nm)/CBP:$Ir(ppy)_2(acac)$ (8 wt%, 15 nm)/2,2′,2″-(1,3,5-Benzinetriyl)-tris(1-phenyl-1-H-benzimidazole) (TPBi) (65 nm)/LiF (0.7 nm)/Al (100 nm), respectively, as shown in Figure 1. Both PhOLEDs exhibit high efficiencies, with the maximum EQEs of 30% and 25% for device 1 and device 2, respectively. They also exhibit low efficiency roll-offs at high current densities, which correspond to 27% and 21% at 10 000 cd m^{-2} in device 1 and device 2, respectively, and very low leakage currents in the low voltage region. Since the same phosphorescent dopant was used in both devices, the higher efficiency in device 1 than device 2 might be due to better balance of electrons and holes in device 1 than device 2.[18]

The injection and turn-on voltages of device 1 are lower than those of device 2. The injection voltage at which the current increases abruptly is 2.0 V, and the turn-on voltage defined as the voltage at 1 cd m^{-2} is 2.3 V in device 1. These values in device 1 are 0.5 V lower than those of device 2, indicating that the charges are efficiently injected from the electrodes and are transported to the emission layer under a low external bias in device 1. Interestingly, the dopant energy levels are differently located relative to the host layers in device 1 and 2. The same phosphorescent dopant, $Ir(ppy)_2(acac)$, was used in both PhOLEDs, but while this dopant is likely to act as both electron trap and hole trap in the CBP based PhOLED (device 2), it will only act as a hole trap in the exciplex forming co-host based PhOLED (device 1). These characteristics will be analyzed and discussed based on the *J–V–L*, transient electroluminescence, and capacitance-voltage characteristics in the next section.

2.2. Determination of Recombination Type in the PhOLEDs

Formation of excitons on the host molecules by Langevin recombination and subsequent energy transfer to the dopant

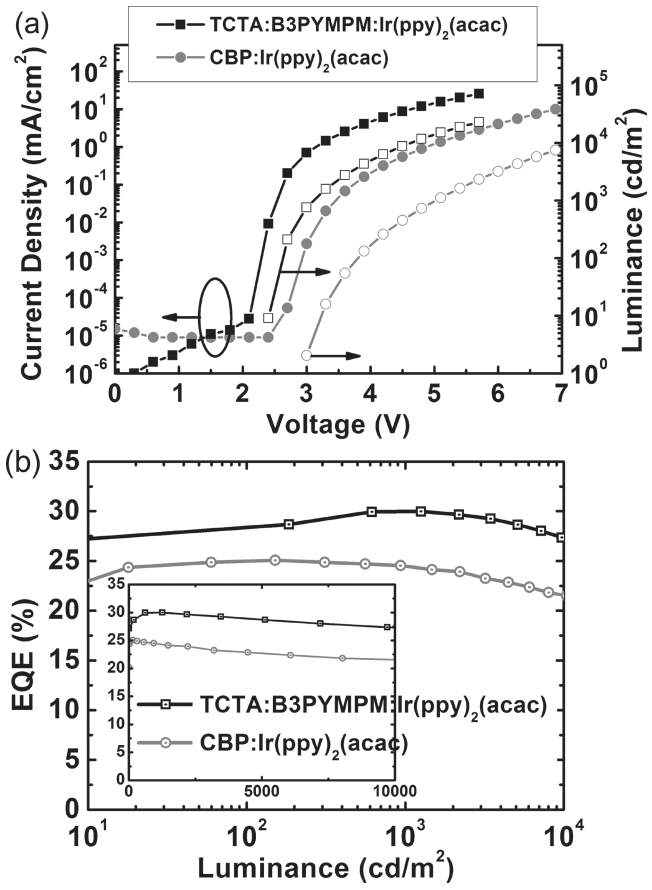

Figure 2. a) Current density-voltage-luminance (*J–V–L*) characteristics and b) (semi-log scale) external quantum efficiency-luminance (η–*L*) characteristics of the TCTA:B3PYMPM:Ir(ppy)$_2$(acac) based PhOLED (device 1) and the CBP:Ir(ppy)$_2$(acac) based PhOLED (device 2). The inset of (b) is depicted in a linear scale.

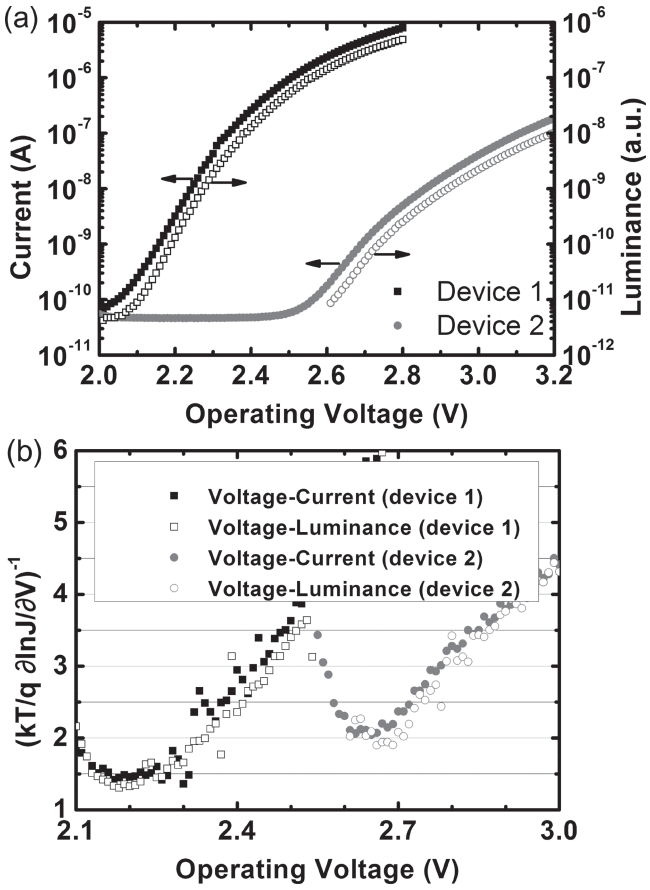

Figure 3. a) *J–V–L* characteristics of the two PhOLEDs in diffusion dominated current region. b) The recombination parameter (η) was calculated from (a) by using Equation 2.

must compete with trap-assisted recombination in the PhOLEDs under electrical pumping, and the different mechanisms will affect the performance of the devices significantly. Bimolecular and trap-assisted recombination of the charge carriers and the emission of excitons are reflected in the *J–V–L* characteristics of the devices, and can be described using the Shockley diode equation in the diffusion dominated region, which is given by[26]

$$J = J_0\left[\exp\left(\frac{qV}{\eta kT}\right) - 1\right] \quad (1)$$

where J_0 denotes the saturation current density, k is the Boltzmann constant, T is the temperature, and q is the unit charge. The recombination parameter (η) in Equation 1 is directly connected to the density of the recombination center, and varies from 1 to 2 depending on the recombination mechanism, with 1 for Langevin recombination and 2 for trap-assisted recombination. This parameter can therefore be used to investigate the major recombination and emission mechanisms in PhOLEDs under electrical excitation.[4,5,27,28] The *J–V–L* characteristics of devices 1 and 2 in the diffusion current region are shown in **Figure 3**a. It is interesting to note that the currents flowed when $V < V_{bi}$ (the built-in potential that corresponds to the flat band condition of the device) because of the diffusion current from the metal reservoir to the organic layer. As a result, the voltages where the currents begin to rise abruptly are 2.0 V and 2.5 V in device 1 and device 2, respectively, and the turn-on voltages where light emission begins to rise are 2.05 V and 2.6 V in device 1 and device 2, respectively. The voltage gaps between injection voltage and turn-on voltage are just 0.05 V and 0.1 V in device 1 and device 2, respectively, because there is a low energy barrier for charge transport inside the devices. Interestingly, the turn-on voltage of 2.05 V in device 1 is much lower than the voltage that corresponds to the emitted photon energy ($V = h\nu / q$) of 2.4 eV of the phosphorescent dopant, Ir(ppy)$_2$(acac), and this is attributed to the device diffusion current.

The recombination parameters of the devices were extracted using Equation 2, and the results are depicted in Figure 3b.

$$\eta = \left(\frac{kT}{q}\frac{\partial \ln J}{\partial V}\right)^{-1} \quad (2)$$

The η value of device 2 approaches 2 in the plateau of the curve, indicating that trap-assisted recombination is dominant

in the system. In contrast, the η value is approximately 1.4 in device 1, indicating the dominance of Langevin recombination in the device. This Langevin recombination dominance indicates that the electron-hole recombination occurs predominantly in the host molecules in device 1; that is, the formation of the exciplex. Although the dopant is energetically located at a hole trap in the device 1, the exciplex forming co-host stimulates exciplex formation in the host, and subsequent energy transfer from the exciplex to the dopant rather than by trap-assisted recombination on dopant molecules, as observed in device 2.

2.3. Transient Electroluminescence (EL) in the PhOLEDs

The recombination characteristics were also analyzed based on the results of the transient EL measurements. **Figure 4** shows the normalized transient EL characteristics of the devices. The voltage pulse width was 100 μs, and the pulse was periodically applied to the devices with a frequency of 100 Hz. The voltage pulse height corresponds to a current density of 10 mA cm^{-1}. The magnitude of the reverse bias after the voltage turn-off was varied up to saturation, as shown in Figure 4. Device 1 showed no difference in the turn-on region and was independent of the magnitude of the reverse bias applied after the pulse turn-off (Figure 4a). In contrast, device 2 showed an initial overshoot in the turn-on region. The overshoot was reduced and the rise time was increased as the reverse bias magnitude increased to −5 V, as shown in Figure 4b. The dependence of the overshoot and the rise time on the reverse bias magnitude after the turn-off in device 2 indicates that residual trapped charges exist after the voltage pulse turn-off for at least 10 μs, until the next pulse is applied. A reverse bias of more than −5 V was required to sweep out the trapped charges in device 2 during the off-time. The luminance overshoot must be related to the recombination of the trapped charges and to the recombination of the injected charges.[29–31]

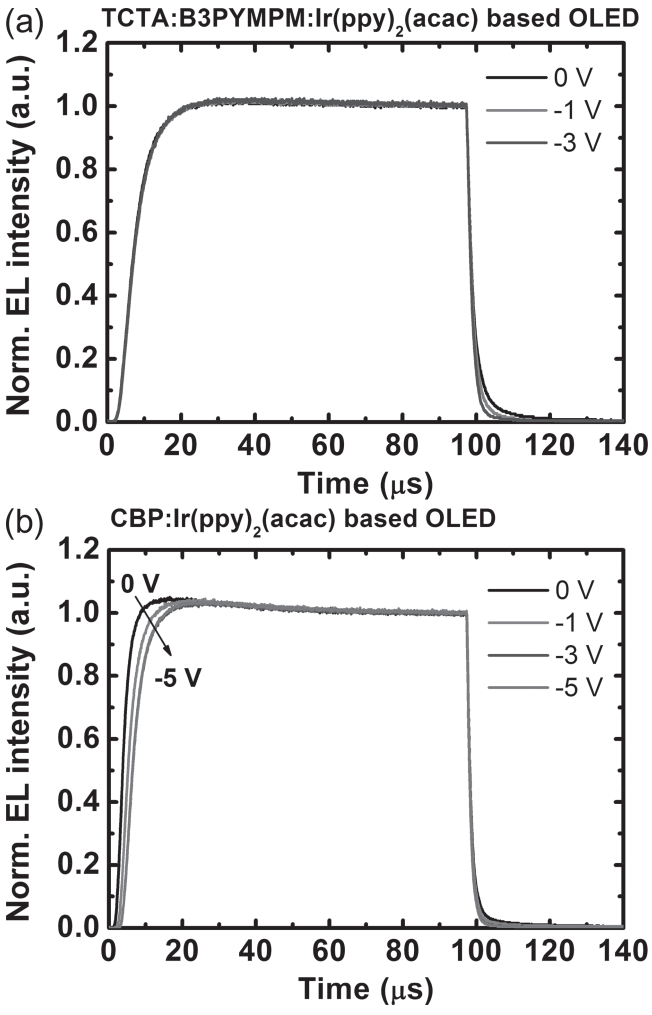

Figure 4. Normalized intensity of transient EL, depending on the reverse bias after turn-off of the voltage pulse in a) device 1 and b) device 2. The voltage pulse width was 100 μs and the pulse frequency was 100 Hz. The voltage pulse height corresponds to a current density of 10 mA cm^{-2}. The magnitude of the reverse bias after the voltage turn-off was gradually increased up to saturation. The initial overshoots caused by the trapped charges in the emission layer are observed only in device 2, and they gradually decrease as the reverse bias magnitude increases.

Further evidence of the existence of trapped charges can be obtained from the frequency dependent behavior of the transient EL, as shown in **Figure 5**. The rise time becomes shorter as the frequency increases in device 2. In contrast, there is no change in the rise time with increasing frequency in device 1. When the excitation pulse frequency increases from 100 to 900 Hz, the number of trapped charges in the EML increases because the trapped charge relaxation time is fixed within the device. As a result, the luminance onset time becomes faster because of the increased numbers of remaining charges as the pulse frequency increases. This phenomenon occurs only in device 2, and not in device 1, supporting the dominance of trap-assisted recombination in device 2 and the dominance of bimolecular Langevin recombination in device 1. The frequency dependence of the transient EL shows a clear difference between a trap-assisted recombination dominant device and a Langevin recombination dominant device.

The transient overshoot or spike at the decay part of the transient EL have also been studied to investigate charge trapping in the small molecule based PhOLEDs, and the results are shown in **Figure 6**. The spike after the voltage turn-off was attributed to recombination of the trapped charges on the dopant site in the EML.[12,13] Interestingly, not only device 1 but also device 2 did not show any overshoot although a considerable amount of carriers were trapped on dopant site in device 2. This behavior can be interpreted based on the hole dominant accumulation on dopant site due to the much deeper hole trap energy than electron trap energy and no existence of electron blocking layers in device 2. The delayed emission or overshoot under reverse bias after turn off of the voltage pulse is generated when both charges are oppositely located and are spatially apart from each other in order to form excitons after recombination of the spatially drifted electrons and holes. However, the overshoots will disappear if only holes are accumulated at the interface or on dopant state owing to the absence of the drifted electrons under reverse bias.[13] As with our previous study,[19] the slow luminance decay up to 350 ns after the voltage pulse turn-off showed independence from the magnitude of the reverse bias voltage in device 1 (Figure 6a). The initially prolonged luminance of

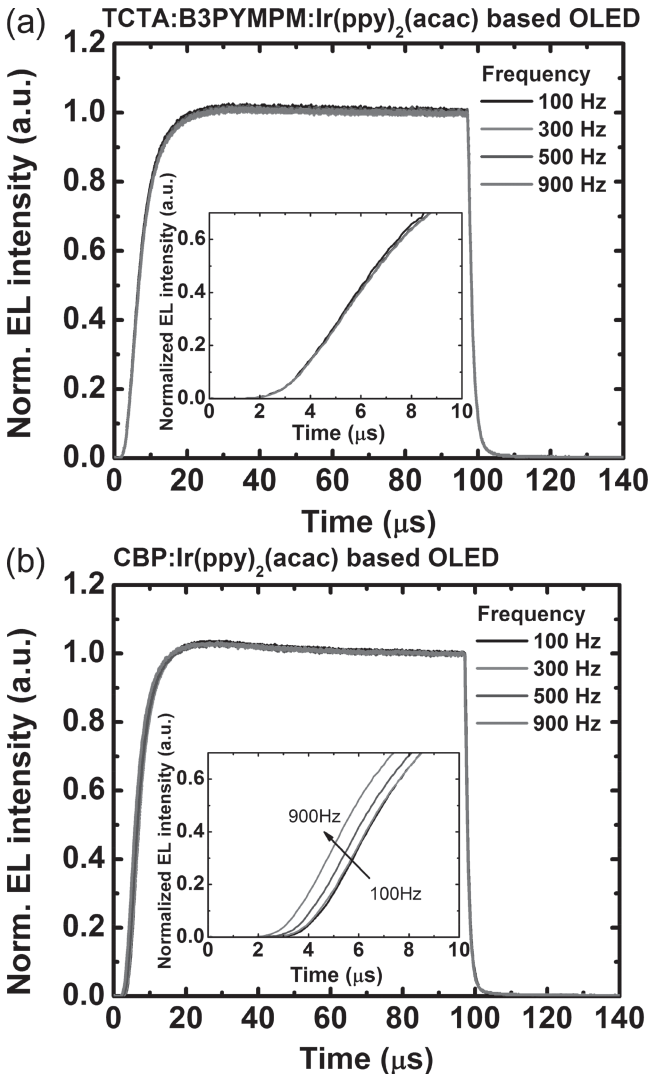

Figure 5. Normalized transient EL intensity depending on the frequency of the voltage pulse in a) device 1, and b) device 2. The voltage pulse width was 100 μs and the voltage pulse height corresponds to a current density of 10 mA cm^{-2}. The frequency of the voltage pulse was gradually increased from 100 Hz to 900 Hz. The initial part of the transient EL was magnified, as shown in the inset. The initial overshoots are still observed and the luminance onset time gradually increases as the frequency increases in device 2. In contrast, there are no changes in device 1 that depend on variation of the frequency.

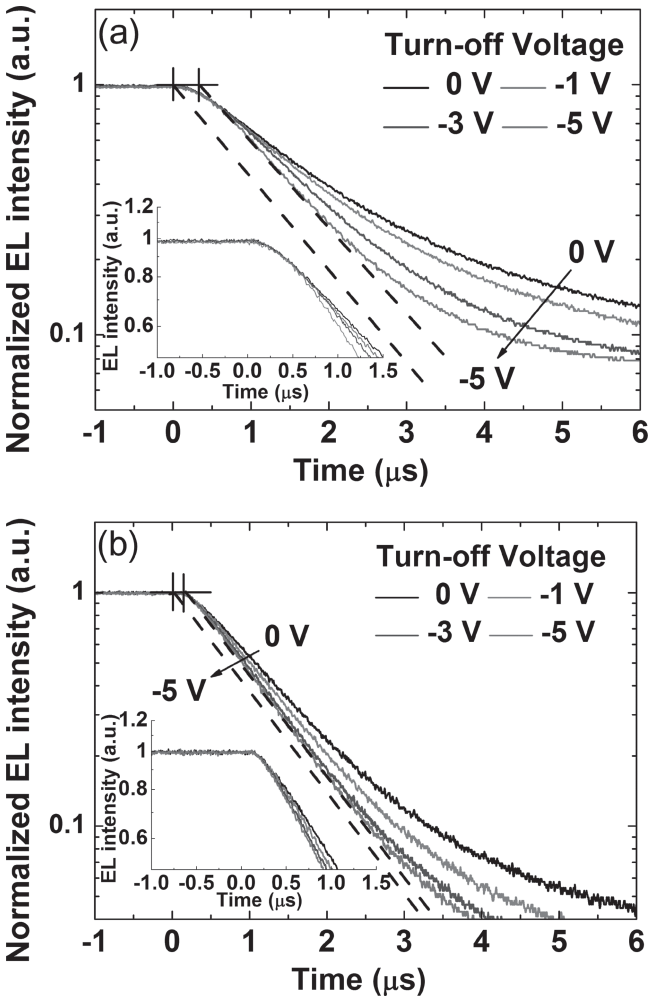

Figure 6. Normalized intensity of the transient EL at the decay part, depending on the reverse bias of the voltage pulse after turn-off in a) device 1, and b) device 2.

up to 350 ns, independent of the reverse bias, is attributed to energy transfer from the neutral host excitons to the dopant, followed by emission from the dopant. Similar behavior was also observed in device 2 (Figure 6b), but the initially prolonged time of the luminance was 140 ns and this value is less than half of that of device 1.

These interpretations of the transient EL characteristics of the devices are supported by the transient behavior of reference devices (device 3 and 4), which have the same structures as device 1 and 2, respectively, but without dopant. **Figure 7** shows the normalized transient EL of device 3 and 4 which were measured using the voltage pulse with the same height, width and the frequency as device 1 and 2. The turn-on of device 3 is a little faster than that of device 1 although the same voltage and current were applied in both devices due to the similar *J–V* characteristics as shown in Figure S1 in Supporting Information, indicating that the hole mobility is reduced in the device 1 compared to device 3 due to the phosphorescent dopant in the EML. However, there are no initial overshoots in the turn-on region of device 1 and 3, suggesting that the charge trapping is not critical in device 1. In contrast, the initial overshoot in the turn-on region of device 2 disappeared in device 4 as shown in Figure 7b due to the absence of the trap site in the EML of device 4. This result clearly proves that the phosphorescent dyes behave as the charge traps in device 2. In addition, the initially prolonged emissions which were observed in device 1 and 2 disappeared in device 3 and 4 owing to the absence of the energy transfer in the fluorescent OLEDs without the phosphorescent dopant. The strong overshoots at ≈ 250 ns after turn off of the voltage pulse especially in device 4 originate from the recombination of remaining charges, indicating that electrons and holes are not confined to the EML in the fluorescent OLED. The overshoot was observed in device 3 but with much less extent because of better confinement of charges in the EML.

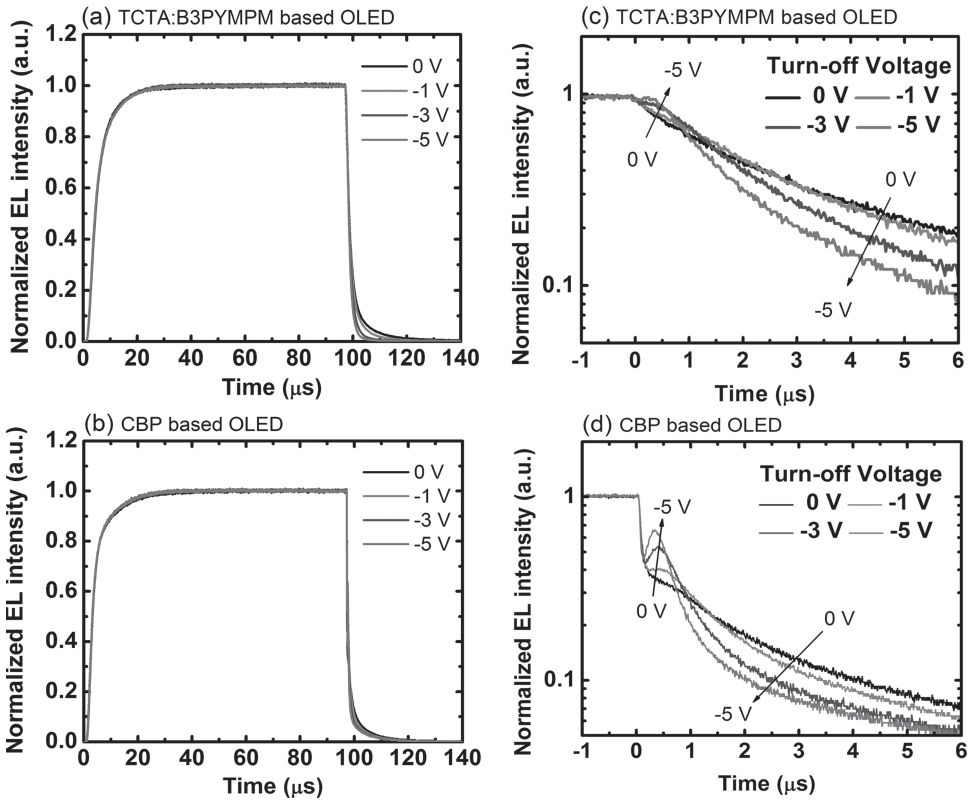

Figure 7. Normalized intensity of the transient EL, depending on the reverse bias of the voltage pulse after turn-off in a) device 3, and b) device 4. Normalized intensity of the transient EL at the decay part, depending on the reverse bias of the voltage pulse after turn-off in c) device 3, and d) device 4. The height of the pulse corresponds to 10 mA cm^{-2} in device 3, and device 4. The voltage pulse width and the frequency of the pulse were 100 μs and 100 Hz, respectively.

Based on the *J–V–L* and transient EL behavior of these devices, we can conclude that Langevin recombination is dominant over trap-assisted recombination in device 1 with its small number of trapped charges. In contrast, trap-assisted recombination is predominant in device 2 because of its large number of trapped holes.

2.4. Analysis of Trapped Charges from C-V Measurement

The trapped charge behavior was also analyzed from the viewpoint of the device capacitance-voltage (*C–V*) characteristics, as shown in **Figure 8**a, where the *J–V* curves have been added for comparison. The capacitance behavior of the two devices showed significant differences. The capacitance of device 1 shows a small peak. This peak starts to increase at approximately 2 V, corresponding to the injection voltage, and reaches a maximum at 2.4 V, followed by a reduction to ground level at around 2.8 V. The existence of the peak in the *C–V* curve indicates the accumulation of the charges inside the device, and these accumulated charges disappear at 2.8 V. The energy diagram shown in Figure 1 and the *J–V* curve of device 1 suggest that some of the diffused charges begin to accumulate at the TAPC/TCTA junction and this accumulation increases up to 2.4 V, which might correspond to the flat band condition. Above that voltage, injection by thermionic emission at the junction becomes efficient for reduction of the accumulated charges. Above 2.8 V, the TAPC/TCTA junction does not behave like an injection barrier any more, which is probably because of the energy barrier lowering effect. Increasing the injected current at voltages above 2.8 V gradually increases the capacitance because of the existence of locally unbalanced electron and hole densities.

In contrast, device 2 showed a much higher peak in the *C–V* curve at a higher voltage than device 1. The capacitance began to slowly rise at 2.5 V up to 3.1 V because of the contribution of the diffusion current, and then increased sharply to a maximum value at 5.4 V. Referring again to the energy diagram shown in Figure 1, the capacitance must arise from the accumulated charges on the dopant molecules, because there are no organic junctions for the injected holes to reach the EML and the energy barrier between TPBi and CBP for the injected electrons to reach the EML is only 0.1 eV. The accumulated charges might be holes, because the hole mobility of the CBP layer (≈10^{-3} cm^2 V^{-1} s^{-1}) is two orders of magnitude higher than the electron mobility of the TPBi layer. In addition, the Poole-Frankel constant (β) of the TPBi layer is more than three times higher than that of the CBP layer, indicating that the electron transport in this device is more sensitive to the external field. Therefore, we can infer that the hole currents are dominant over the electron currents to an extent that the extra holes are accumulated in the EML, particularly on the

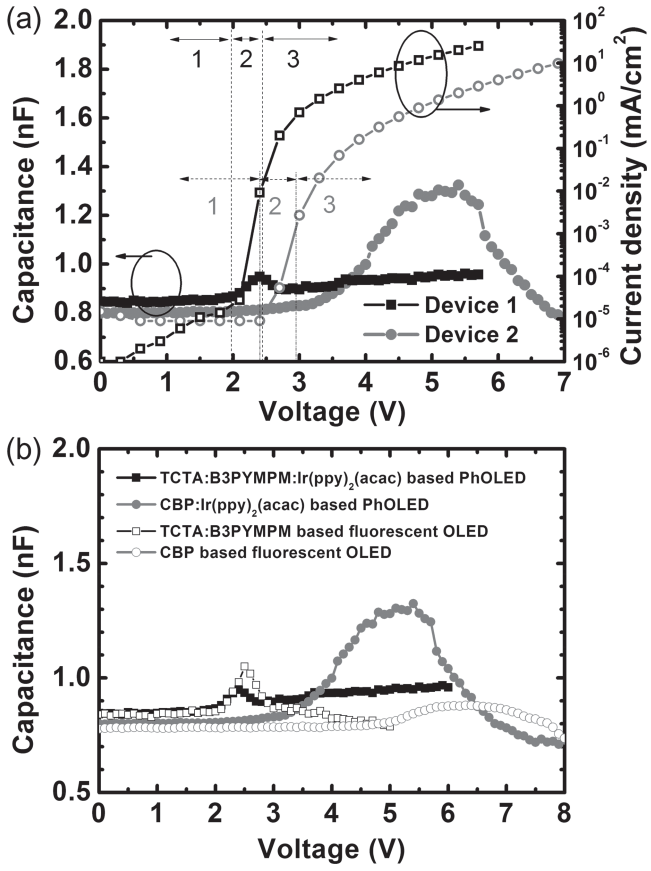

Figure 8. a) Capacitance-voltage (*C–V*) plots and current density-voltage (*J–V*) curves for the two different PhOLEDs. The *J–V* curves of the PhOLEDs were classified into the following three regions: 1) Ohmic current, 2) diffusion dominated current, and 3) drift dominated current regions. b) *C–V* plots of two PhOLEDs and two fluorescent OLEDs.

dopant molecules, during light emission at up to 5.4 V. As the bias then increases to more than 5.4 V, the accumulated holes are rapidly annihilated by recombination with the injected electrons at the high bias, because of the increased mobility from the high β value. The *C–V* characteristics in device 2 are similar to the characteristics that were previously reported when using bilayer structured OLEDs.[32–34]

Similar C–*V* characteristics of device 3 (no phosphorescent dye) with device 1 (with phosphorescent dye) and much lower the peak of the capacitance in device 4 (no phosphorescent dye) than device 2 (with phosphorescent dye) confirm that charges are accumulated at the TAPC/TCTA interface in device 1 and on dopant site in device 2 as shown in Figure 8b, respectively.

Based on the *J–V–L*, transient EL, and *C–V* characteristics, the different recombination behaviors of the two PhOLEDs were elucidated. Major factor for the different recombination behaviors is the relative energy level of the dopant and host materials. In contrast to single host, the energy gap of the exciplex forming co-host is defined as the energy level difference between highest occupied molecular orbital (HOMO) level of donor and lowest unoccupied molecular orbital (LUMO) level of acceptor molecule. In addition, the energy gap between triplet and singlet energy level of the exciplex forming host is very close so that it can be considered as an advanced quasi-host material.[35–38] Therefore, the energy gap of the exciplex can be easily adjusted and the trap energy of the dopant is able to be reduced by selecting proper donor and acceptor molecules. The energy transfer from the exciplex state to the dopant state is also achieved due to low energy mismatch between them.[18,19,38]

Different recombination mechanisms in phosphorescent OLEDs influence on the *J–V* characteristics significantly due to the existence of the phosphorescent dye as shown in Figure S1 in Supporting Information. The *J–V* characteristics in Langevin recombination dominant phosphorescent OLEDs are almost the same as the dopant free devices (Figure S1a, Supporting Information). In contrast, in device 2 where the trap assisted recombination is dominant, the accumulated holes enhance the local field in the EML to enhance the electron injection. As a result, improved current flow and EQE of device 2 were demonstrated as shown in Figure 2 and Figure S1 compared to the fluorescent OLED without dopant.

3. Conclusions

In summary, the *J–V* characteristics in the diffusion current region and the transient EL and C–V measurements clearly demonstrated that the Langevin recombination and energy transfer process are dominant over trap-assisted recombination in the green PhOLED with the exciplex forming co-host system. The exciplex forming system can be considered to be a quasi-host that has its HOMO and LUMO levels as the HOMO of the hole transport material (donor) and the LUMO of the electron transport material (acceptor). In addition, its triplet energy level is almost the same as that of the singlet, meaning that we can select a quasi-host such that its HOMO-LUMO gap is very close to the phosphorescent dopant. In that way, the trap energy of the dopant can be minimized, easing the Langevin recombination process, as in the case of this study of the exciplex forming host. The low polaron density combined with the efficient energy transfer from exciplex to dopant results in a low efficiency roll–off in the device. In contrast, single host systems generally have a large singlet–triplet energy gap, such that a host with a large HOMO–LUMO gap must have a higher triplet energy than the triplet gap of the phosphorescent dopant. Therefore, single host systems generally have high trap energies, which results in the dominance of trap-assisted recombination in the PhOLEDs.

4. Experimental Section

High efficiency PhOLEDs with the following structures were fabricated to investigate the charge recombination mechanisms: ITO (70 nm)/TAPC (75 nm)/TCTA (10 nm)/TCTA:B3PYMPM:bis(2-phenylpyridine) iridium(III)-acetylacetonate [$Ir(ppy)_2(acac)$] (1:1 molar ratio and 8 wt%, 30 nm)/B3PYMPM (40 nm)/LiF (0.7 nm)/Al (100 nm) (device 1), and ITO (70 nm)/MoO_3 (1 nm)/CBP (90 nm)/CBP:$Ir(ppy)_2(acac)$ (8 wt%, 15 nm)/TPBi (65 nm)/LiF (0.7 nm)/Al (100 nm) (device 2). The structures of the devices, the HOMO and LUMO levels, and the chemical structures of the organic materials are shown in Figure 1. All layers were thermally deposited on a pre-cleaned glass substrate patterned with ITO under a base pressure of 5×10^{-7} Torr in evaporation chambers without breaking the vacuum. The active area of both devices

was 2 mm × 2 mm. At the end of the fabrication process, all devices were encapsulated with glass lids using ultraviolet (UV)-curing epoxy resin in a glove box filled with nitrogen gas, and a desiccant film was also attached inside the glass lid. The *J–V–L* characteristics of the PhOLEDs were measured using a semiconductor parameter analyzer (Keithley 237) and a spectrophotometer (Photo Research PR-650). To determine the recombination parameter in the diffusion current region, a programmable source meter (Keithley 2400) and a Si photodiode (1835C, Newport) were also used. The time-resolved EL intensity was obtained using a pulse generator (Agilent 8114A) and a spectrometer (SpectraPro-300i) connected to a photomultiplier tube (Acton Research, PD-438). The voltage pulses that were applied to the device corresponded to a current density of 10 mA cm^{-2} with a pulse width of 100 μs, and the frequencies of 100–900 Hz. The detection wavelength was 520 nm, which corresponds to the peak wavelength of $Ir(ppy)_2(acac)$ emission. All signals were detected and integrated more than 1000 times using an oscilloscope (Agilent 54642A). The voltage applied to each OLED was measured over a 1 MΩ resistance that was parallel to the OLED.

Supporting Information

Supporting Information is available from the Wiley Online Library or from the author.

Acknowledgements

This work was supported by the Industrial strategic technology development program [10035225, Development of core technology for high performance AMOLED on plastic] funded by MKE/KEIT.

Received: October 8, 2013
Revised: February 27, 2014
Published online: April 22, 2014

[1] P. Langevin, *Ann. Chim. Phys.* **1903**, *28*, 122.
[2] R. N. Hall, *Phys. Rev.* **1952**, *87*, 387.
[3] W. Shockley, W. Read Jr., *Phys. Rev.* **1952**, *87*, 835.
[4] M. Kuik, L. J. A. Koster, G. A. H. Wetzelaer, P. W. M. Blom, *Phys. Rev. Lett.* **2011**, *107*, 256805.
[5] M. Kuik, H. T. Nicolai, M. Lenes, G.-J. A. H. Wetzelaer, M. Lu, P. W. M. Blom, *Appl. Phys. Lett.* **2011**, *98*, 093301.
[6] P. A. Lane, L. C. Palilis, D. F. O'Brien, C. Giebeler, A. J. Cadby, D. G. Lidzey, A. J. Campbell, W. Blau, D. D. C. Bradley, *Phys. Rev. B* **2001**, *63*, 235206.
[7] J. Mäkinen, I. G. Hill, Z. H. Kafafi, *J. Appl. Phys.* **2002**, *92*, 1598.
[8] X. Gong, J. C. Ostrowski, D. Moses, G. C. Bazan, A. J. Heeger, *Adv. Funct. Mater.* **2003**, *13*, 439.
[9] A. J. Sandee, C. K. Williams, N. R. Evans, J. E. Davies, C. E. Boothby, A. Köhler, R. H. Friend, A. B. Holmes, *J. Am. Chem. Soc.* **2004**, *126*, 7041.
[10] G. He, M. Pfeiffer, K. Leo, M. Hofmann, J. Birnstock, R. Pudzich, J. Salbeck, *Appl. Phys. Lett.* **2004**, *85*, 3911.
[11] H. Yersin, *Top. Curr. Chem.* **2004**, *241*, 1.
[12] R. Liu, Z. Gan, R. Shinar, J. Shinar, *Phys. Rev. B* **2011**, *83*, 245302.
[13] C. Weichsel, L. Burtone, S. Reineke, S. I. Hintschich, M. C. Gather, K. Leo, B. Lüssem, *Phys. Rev. B* **2012**, *86*, 075204.
[14] M. A. Baldo, S. Lamansky, P. E. Burrows, M. E. Thompson, S. R. Forrest, *Appl. Phys. Lett.* **1999**, *75*, 4.
[15] M. A. Baldo, M. E. Thompson, S. R. Forrest, *Nature* **2000**, *403*, 750.
[16] Z. G. Gao, B. X. Mi, H. L. Tam, K. W. Cheah, C. H. Chen, M. S. Wong, S. T. Lee, C. S. Lee, *Adv. Mater.* **2008**, *20*, 774.
[17] W. S. Jeon, T. J. Park, S. Y. Kim, R. Pode, J. Jang, J. H. Kwon, *Org. Electron.* **2009**, *10*, 240.
[18] S.-Y. Kim, W.-I. Jeong, C. Mayr, Y.-S. Park, K.-H. Kim, J.-H. Lee, C.-K. Moon, W. Brütting, J.-J. Kim, *Adv. Funct. Mater.* **2013**, *23*, 3896.
[19] Y.-S. Park, S. Lee, K.-H. Kim, S.-Y. Kim, J.-H. Lee, J.-J. Kim, *Adv. Funct. Mater.* **2013**, *23*, 4914.
[20] M. G. Helander, Z. B. Wang, J. Qiu, M. T. Greiner, D. P. Puzzo, Z. W. Liu, Z. H. Lu, *Science* **2011**, *332*, 944.
[21] Z. B. Wang, M. G. Helander, J. Qiu, D. P. Puzzo, M. T. Greiner, Z. W. Liu, Z. H. Lu, *Appl. Phys. Lett.* **2011**, *98*, 073310.
[22] M. A. Baldo, C. Adachi, S. R. Forrest, *Phys. Rev. B* **2000**, *62*, 10967.
[23] J. Kalinowski, W. Stampor, J. Mężyk, M. Cocchi, D. Virgili, V. Fattori, P. Di Marco, *Phys. Rev. B* **2002**, *66*, 235321.
[24] S. Reineke, K. Walzer, K. Leo, *Phys. Rev. B* **2007**, *75*, 125328.
[25] D. Song, S. Zhao, Y. Luo, H. Aziz, *Appl. Phys. Lett.* **2010**, *97*, 243304.
[26] W. Shockley, *Bell Syst. Tech.* **1949**, *J 28*, 435.
[27] P. Ashburn, D. Morgan, M. Howes, *Solid-State Electron.* **1975**, *18*, 569.
[28] G. A. H. Wetzelaer, M. Kuik, H. T. Nicolai, P. W. M. Blom, *Phys. Rev. B* **2011**, *83*, 165204.
[29] V. Savvateev, A. Yakimov, D. Davidov, *Adv. Mater.* **1999**, *11*, 519.
[30] C. W. Ma, O. Lengyel, J. Kovac, I. Bello, C. S. Lee, S. T. Lee, *Chem. Phys. Lett.* **2004**, *397*, 87.
[31] H. Kajii, K. Takahashi, J.-S. Kim, Y. Ohmori, *J. Appl. Phys.* **2006**, *45*, 3721.
[32] W. Brütting, H. Riel, T. Beierlein, W. Riess, *J. Appl. Phys.* **2001**, *89*, 1704.
[33] S. Nowy, W. Ren, A. Elschner, W. Lövenich, W. Brütting, *J. Appl. Phys.* **2010**, *107*, 054501.
[34] K. S. Yook, S. O. Jeon, S.-Y. Min, J. Y. Lee, H.-J. Yang, T. Noh, S.-K. Kang, T.-W. Lee, *Adv. Funct. Mater.* **2010**, *20*, 1797.
[35] Y.-S. Park, W.-I. Jeong, J.-J. Kim, *J. Appl. Phys.* **2011**, *110*, 124519.
[36] K. Goushi, K. Yoshida, K. Sato, C. Adachi, *Nat. Photonics* **2012**, *6*, 253.
[37] Y.-S. Park, K.-H. Kim, J.-J. Kim, *Appl. Phys. Lett.* **2013**, *102*, 153306.
[38] S. Lee, K.-H. Kim, D. Limbach, Y.-S. Park, J.-J. Kim, *Adv. Funct. Mater.* **2013**, *23*, 4105.